Supporting Information

for

Visible–Light–Driven Photocatalytic H_2 Evolution over CdZnS Nanocrystal Solid Solutions: Interplay of Twin Structures, Sulfur Vacancies and Sacrificial Agents

Hai–Bo Huang[a,b,c], Zhi–Bin Fang[a], Kai–Yu[b], Jian Lü[a,b,*] and Rong Cao[a,*]

[a] State Key Laboratory of Structural Chemistry, Fujian Institute of Research on the Structure of Matter, Chinese Academy of Sciences, Fuzhou 350002, P.R. China; [b] Fujian Provincial Key Laboratory of Soil Environmental Health and Regulation, College of Resources and Environment, Fujian Agriculture and Forestry University, Fuzhou 350002, P.R. China; [c] University of Chinese Academy of Sciences, Beijing 100049, P.R. China.

*Corresponding authors. E–mail: jian_lu_fafu@163.com (J.L.); rcao@fjirsm.ac.cn (R.C.).

Number of pages: 19

Number of tables: 5

Number of figures: 12

Experimental Characterizations

Powder X–ray diffraction (PXRD) patterns were collected using a Rigaku Miniflex 600 X–ray diffractometer with Cu Kα radiation (λ = 0.154 nm). Scanning electron microscopy (SEM) images were photographed by using a JSM6700–F with a working voltage of 10 kV. Transmission electron microscopy (TEM) and high resolution TEM (HR–TEM) images were recorded by using an FEIT 20 working at 200 kV. X–ray photoelectron spectroscopy (XPS) measurements were performed on a Thermo Fisher ESCALAB 250Xi spectrometer with Al Kα X–ray source (15 kV, 10 mA). In order to compensate effects related to charge shifts C 1s peak at 284.6 eV was used as internal standard. Diffuse reflectance spectra (DRS) were recorded on a Shimadzu UV–vis spectrophotometer (UV–2550) with $BaSO_4$ as the background. The photoluminescence (PL) spectra and Time–resolved photoluminescence (TR–PL) decay spectra were collected on a FLS 980 fluorometer spectrometer at room temperature. Electron spin resonance (ESR) spectra were recorded on a Bruker E500 spectrometer. Cd and Zn contents were determined by Jobin Yvon Ultima 2 inductively coupled plasma (ICP) atomic emission spectrometer.

Photoelectrochemical tests

The photoelectrochemical test was performed on an electrochemical analyzer (Zahner, Germany) in a standard three–electrode cell. The Na_2SO_4 (0.2 M, pH = 6.8) aqueous solution was used as supporting electrolyte. The working electrodes were prepared by dropping 100 μL photocatalyst suspension (5 mg photocatalyst powder was added into 50 μL 5% Nafion and 1.0 mL ethanol mixed solution and then sonication for 1 h) onto the indium tin oxide (ITO) glass surface with a coated area of 1 × 1 cm^2, and finally dried at 50 °C in an oven. The counter and reference electrodes were Pt

mesh and Ag/AgCl, respectively.[S1,S2] The transient photocurrent measurements were recorded under the visible light illumination and a 300 W Xe–lamp equipped with an optical cutoff filter of 420 nm was employed for the visible–light excitation. Electrochemical impedance spectroscopy (EIS) plots were collected at off circuit potentials, with the frequency ranging from 100 kHz to 0.1 Hz and modulation amplitude of 5 mV. Mott–Schottky curves were recorded in dark with a voltage of 5 mV at frequencies of 1.0 kHz, respectively.[S3]

Computational details

The configurations and electronic structures were carried out using density functional theory (DFT) implemented via the Vienna Ab–initio Simulation Package (VASP). The generalized gradient approximation (GGA) functional and Perdew−Burke−Ernzerhof (PBE) functional were used for the electronic exchange and correlation effects. The electron occupancies were determined according to Fermi scheme with an energy smearing of 0.1 eV. Geometries were optimized until the energy and the force were converged to 1.0×10^{-6} eV/atom and 0.01 eV/Å, respectively. An energy cutoff was set as 400 eV for the plane–wave expansion of the electronic wavefunction. Due to the existence of the magnetic atoms, spin polarization was considered in all the calculations.

There are two kinds of $Cd_{0.6}Zn_{0.4}S$ solid solution structures, i.e., zinc–blende (cubic phase) and wurtzite (hexagonal phase). To construct the zinc–blende $Cd_{0.6}Zn_{0.4}S$ structure, we first built a ($1 \times 1 \times 5$) supercell along the c axis of primitive cell (cubic, F4–3M), which contains ten Cd atoms, ten Zn atoms, and twenty S atoms. Then, two Zn atoms are substituted by two Cd atoms randomly in order to obtain the $Cd_{0.6}Zn_{0.4}S$ ratio. We consider four different configurations of zinc–blende $Cd_{0.6}Zn_{0.4}S$ with 40 atoms, as shown in Figure S6. We found that the total energies of four different configurations of the zinc–blende $Cd_{0.6}Zn_{0.4}S$ in Figure S7 are very close, i.e., –130.88 eV, –130.95

eV, –130.94 eV, and –130.92 eV, respectively. This shows that the arrangement of the substitutional atoms (Cd and Zn) in the solid solution can be considered randomly. Thus, we chose the relatively more stable configuration b for the further investigation. Similarly, to construct the wurtzite $Cd_{0.6}Zn_{0.4}S$ structure, we also built a (1×1×5) supercell along the c axis of primitive cell (hexagonal), which contains five Cd atoms, five Zn atoms, and ten S atoms. Then, one Zn atom is substituted by one Cd atom randomly in order to obtain the $Cd_{0.6}Zn_{0.4}S$ ratio and the chosen configuration is shown in Figure S8. To keep the consistent atom numbers with zinc–blende $Cd_{0.6}Zn_{0.4}S$, a ($2 \times 1 \times 1$) supercell along the a axis is further built and the total energy of the obtained wurtzite $Cd_{0.6}Zn_{0.4}S$ configuration is –130.09 eV, which is much higher than the total energy of zinc–blende $Cd_{0.6}Zn_{0.4}S$. Thus, the zinc–blende $Cd_{0.6}Zn_{0.4}S$ structure is more stable than the wurtzite structure.

For the zinc–blende $Cd_{0.6}Zn_{0.4}S$ structures, two stable terminal surfaces of (110) and (111) were chosen. To model the $Cd_{0.6}Zn_{0.4}S$(110) and (111) surfaces, a 5×1 slab with 4 layers and 40 atoms was employed. A vacuum region of 15 Å was introduced to avoid the interactions between the periodic slabs. The positions of all atoms were allowed to relax. The $3 \times 3 \times 3$ Monkhorst–Pack grid was used for the $Cd_{0.6}Zn_{0.4}S$ primitive cell, and a $3 \times 3 \times 1$ grid was used for the bulk $Cd_{0.6}Zn_{0.4}S$ supercells, the (110) and (111) surfaces. Besides, we also consider the two surfaces with surfur vacancy. The detailed configurations are shown in Figure S10. The corresponding total and partial density of states (TDOS and PDOS) of bulk $Cd_{0.6}Zn_{0.4}S$, perfect $Cd_{0.6}Zn_{0.4}S$(110) and (111) surfaces, and $Cd_{0.6}Zn_{0.4}S$(110) and (111) surfaces with sulfur vacancy are shown in Figures S9 and S11. It is found that the electronic structures of these $Cd_{0.6}Zn_{0.4}S$ solid solution have a configuration–independent feature. The charge density difference maps of zinc–blende perfect $Cd_{0.6}Zn_{0.4}S$ (110) and (111) surfaces, and the two surfaces with sulfur vacancy are shown in Figure 6

and S12. It is seen that the sulfur vacancy induces the loss of electron accumulation.

References

(S1) H. B. Huang, Y. Wang, W. B. Jiao, F. Y. Cai, M. Shen, S. G. Zhou, H. L. Cao, J. Lü and R. Cao, *ACS Sustain. Chem. Eng.*, 2018, **6**, 7871−7879.

(S2) X. Q. Hao, J. Zhou, Z. W. Cui, Y. C. Wang, Y. Wang and Z. G. Zou, *Appl. Catal. B-Environ.*, 2018, **229**, 41–51.

(S3) H. Liu, C. Y. Xu, D. D. Li and H. L. Jiang, *Angew. Chem. Int. Ed*., 2018, **57**, 5379–5383.

(S4) M. Zhou, S. B. Wang, P. J. Yang, C. J. Huang and X. C. Wang, *ACS Catal.*, 2018, **8**, 4928–4936.

(S5) M. C. Liu, L. Z. Wang, G. Q. Lu, X. D. Yao and L. J. Guo, *Energy Environ. Sci*., 2011, **4**, 1372–1378.

(S6) F. Del Valle, A. Ishikawa, K. Domen, J. A. V. de la Mano, M. C. Sánchez–Sánchez, I. D. González, S. Herreras, N. Mota, M. E. Rivas, M. C. A. Galván, J. L. G. Fierro and R. M. Navarro, *Catal. Today*, 2009, **143**, 51−56.

(S7) J. Yu, J. Zhang and M. Jaroniec, *Green Chem.*, 2010, **12**, 1611−1614.

(S8) Q. Li, H. Meng, P. Zhou, Y. Q. Zheng, J. Wang, J. G. Yu and J. R. Gong, *ACS Catal.*, 2013, **3**, 882−889.

(S9) Y. G. Yu, G. Chen, Y. S. Zhou, Y. Wang and C. Wang, *New J. Chem.*, 2014, **38**, 486−489.

(S10) M. Q. Chen, P. X. Wu, Y. J. Zhu, S. S. Yang, Y. H. Lu and Z. Lin, *Int. J. Hydrogen Energ.*, 2018, **43**, 10938–10949.

(S11) C. Y. Zhang, H. H. Liu, W. N. Wang, H. S. Qian, S. C. Wang, Z. B. Zha, Y. J. Zhong and Y. Hu, *Appl. Catal. B-Environ.*, 2018, **239**, 309−316.

(S12) C. Zeng, Y. M. Hu, T. R. Zhang, F. Dong, Y. H. Zhang and H. W. Huang, *J. Mater. Chem. A*, 2018, **6**, 16932−16942.

(S13) W. Zhong, X. Huang, Y. Xu and H. G. Yu, *Nanoscale*, 2018, **10**, 19418−19426.

(S14) J. G. Song, H. T. Zhao, R. R. Sun, X. Y. Li and D. J. Sun, *Energy Environ. Sci.*, 2017, **10**, 225−235.

Table Caption

Table S1. Classification and concentration of the used sacrificial agents and the pH value of reaction system.

Table S2. Time–resolved photoluminescence decay parameters of $Cd_xZn_{1-x}S$ nanocrystal solid solutions (NCSSs).

Table S3. Photocatalytic H_2–production over $Cd_{0.6}Zn_{0.4}S$ NCSSs and different samples.

Table S4. Contents of Cd and Zn, Band gap energy (E_g), flat band potential (E_{fb}), and H_2–evolution rate of the $Cd_xZn_{1-x}S$ (x = 0, 0.2, 0.4, 0.6, 0.8 and 1.0).

Table S5. Data for the calculation of apparent quantum yield (AQY) of the $Cd_{0.6}Zn_{0.4}S$ photocatalyst.

Figure Caption

Figure S1. XPS survey spectra of $Cd_xZn_{1-x}S$ NCSSs.

Figure S2. (a) TEM; (b) HR–TEM; (c) SEAD patterns of CdS; (d) TEM; (e) HR–TEM; (f) SEAD patterns of ZnS.

Figure S3. (a) Blank experiments; (b) photocatalytic H_2 evolution using Na_2S/Na_2SO_3 and lactic acid as sacrificial agents of CdS and ZnS; (c) amines; and (d) alcohols concentration on the H_2–evolution rate of $Cd_{0.6}Zn_{0.4}S$ NCSSs.

Figure S4. The $Cd_{0.6}Zn_{0.4}S$ catalyst after cyclic experiment of (a) PXRD patterns; (b) TEM; (c) HR-TEM; and (d) elemental mapping.

Figure S5. (a) PXRD patterns; and (b) photocatalytic H_2 evolution using Na_2S/Na_2SO_3 as sacrificial agents of $Cd_{0.6}Zn_{0.4}S$–80, $Cd_{0.6}Zn_{0.4}S$, $Cd_{0.6}Zn_{0.4}S$–600.

Figure S6. Measurement of power of Xe-lamp by digital optical controller (using the 420 nm band pass filter): (a) blank; (b) center; (c) up; (d) down; (e) left; (f) right.

Figure S7. Configurations of the zinc–blende (cubic phase) $Cd_{0.6}Zn_{0.4}S$ NCSS.

Figure S8. Configurations of the wurtzite (hexagonal phase) $Cd_{0.6}Zn_{0.4}S$ NCSS.

Figure S9. The total density of states (TDOS) and partial density of states (PDOS) of the (a) zinc–blende and (b) wurtzite $Cd_{0.6}Zn_{0.4}S$ NCSS.

Figure S10. The zinc–blende perfect $Cd_{0.6}Zn_{0.4}S$ (110) and (111) surfaces (a) and (c) or defective (with sulfur vacancy) (b) and (d).

Figure S11. TDOS and PDOS of the zinc–blende perfect $Cd_{0.6}Zn_{0.4}S$ (110) and (111) surfaces (a) and (c) or defective (with sulfur vacancy) (b) and (d) corresponding to **Figure S10**.

Figure S12. The charge density difference maps of zinc–blende perfect $Cd_{0.6}Zn_{0.4}S$ (111) surface, and (111) surface with sulfur vacancy (Blue region represent the electron accumulation, Yellow region represent the electron deletion, Isosurfaces = 0.02 eV).

Table S1

Sacrificial reagents	Concentration	pH[a]
Na_2S/Na_2SO_3	0.175 M / 0.125 M	11.8
	0.35 M / 0.25 M	12.3
	0.70 M / 0.50 M	13.9
Carboxylic acid		
Lactic acid	10% (vol%)	1.9
Methane acid	10% (vol%)	1.6
Ascorbic acid	0.75 M	2.4
Alcohols		
Methanol	10% (vol%)	6.4
Glycol	10% (vol%)	6.3
Glycerin	10% (vol%)	6.2
Amines		
Triethanolamine	10% (vol%)	10.8
Ethanediamine	10% (vol%)	10.7
Methylamine	10% (vol%)	10.5

[a] Measured by a pH meter at room temperature (about 20 °C).

Table S2

photocatalysts	Lifetime <τ> (ns)	Pre–exponential factor A%	<τ_{ave}> (ns)[b]
$Cd_{0.2}Zn_{0.8}S$	τ_1 = 8.46 τ_2 = 9.50	A_1 = 37.87 A_2 = 62.13	9.13
$Cd_{0.4}Zn_{0.6}S$	τ_1 = 6.03 τ_2 = 7.24	A_1 = 22.23 A_2 = 77.77	7.01
$Cd_{0.6}Zn_{0.4}S$	τ_1 = 4.62 τ_2 = 4.90	A_1 = 30.55 A_2 = 69.45	4.82
$Cd_{0.8}Zn_{0.2}S$	τ_1 = 6.63 τ_2 = 7.31	A_1 = 25.28 A_2 = 74.72	7.15

[b] Time–resolved photoluminescence decay curves were fitted by using the three–expontial fitting method. Average lifetime <τ_{ave}> was determined by using the following equation: $<\tau_{ave}>=\sum_{i=1}^{i=n} A_i\tau_i^2 \Big/ \sum_{i=1}^{i=n} A_i\tau_i$ according to the literature [S4]

Table S3

Photocatalyst	Incident light (nm)	Light source	Sacrificial agent	Activity (μmol h^{-1} g^{-1})	Ref
$Cd_{0.5}Zn_{0.5}S$	>430	300W (Xe)	0.35 M Na_2S / 0.25 M Na_2SO_3	17900	(S5)
$Cd_{0.7}Zn_{0.3}S$	Visible light	300W (Xe)	0.05 M Na_2S / 0.02 M Na_2SO_3	Ca.350	(S6)
$Cd_{0.8}Zn_{0.2}S$	>400	350W (Xe)	0.1 M Na_2S / 0.04 M Na_2SO_3	2128	(S7)
$Cd_{0.5}Zn_{0.5}S$	>400	350W (Xe)	Na_2S / 0.31 M Na_2SO_3	7420	(S8)
$Cd_{0.6}Zn_{0.4}S$-0.6	>400	300W (Xe)	0.4 M Na_2S / 0.6 M Na_2SO_3	24000	(S9)
$Cd_{0.5}Zn_{0.5}S$(en)	>420	300W (Xe)	0.35 M Na_2S / 0.25 M Na_2SO_3	13539	(S10)
DS-$Zn_{0.46}Cd_{0.54}S$	>420	300W (Xe)	0.35 M Na_2S / 0.25 M Na_2SO_3	4100	(S11)
$Cd_{0.5}Zn_{0.5}S$	>420	300W (Xe)	0.35 M Na_2S / 0.25 M Na_2SO_3	330	(S12)
$Cd_{0.6}Zn_{0.4}S$	UV light	300W (Xe)	0.35 M Na_2S / 0.25 M Na_2SO_3	717.19	(S13)
$Cd_{0.5}Zn_{0.5}S$	>420	300W (Xe)	0.75 M ascorbic acid	42000	(S14)
$Cd_{0.6}Zn_{0.4}S$	>420	300W (Xe)	0.35 M Na_2S / 0.25 M Na_2SO_3	42660	This work

Table S4

photocatalysts	Cd content	Zn content	E_g (eV)	E_{fb} (V)	H_2 evolution (μmol/g/h) [a]	H_2 evolution (μmol/g/h) [b]
ZnS	0	1.0	3.56	–1.04	20.5	143.2
$Cd_{0.2}Zn_{0.8}S$	0.19	0.81	2.54	–0.77	21313.6	1830.5
$Cd_{0.4}Zn_{0.6}S$	0.41	0.59	2.51	–0.75	32900.3	5180.6
$Cd_{0.6}Zn_{0.4}S$	0.63	0.37	2.47	–0.72	42660.0	8920.0
$Cd_{0.8}Zn_{0.2}S$	0.80	0.20	2.38	–0.66	19348.6	5316.4
CdS	1.0	0	2.28	–0.62	61.7	1987.6

[a] 0.35 M Na_2S / 0.25 M Na_2SO_3 aqueous solution as sacrifice agent; [b] 10% lactic acid aqueous solution as sacrifice agent.

Table S5

Wavelength (nm)	**Irradiance (W * π cm^{-2})**	**H_2–evolution (μmol h^{-1} 5mg^{-1})**	**AQY (%)**
420	0.45	80.1	17.6
450	0.46	52.4	10.5
475	0.48	40.4	7.4
520	0.49	20.2	3.3

Figure S1

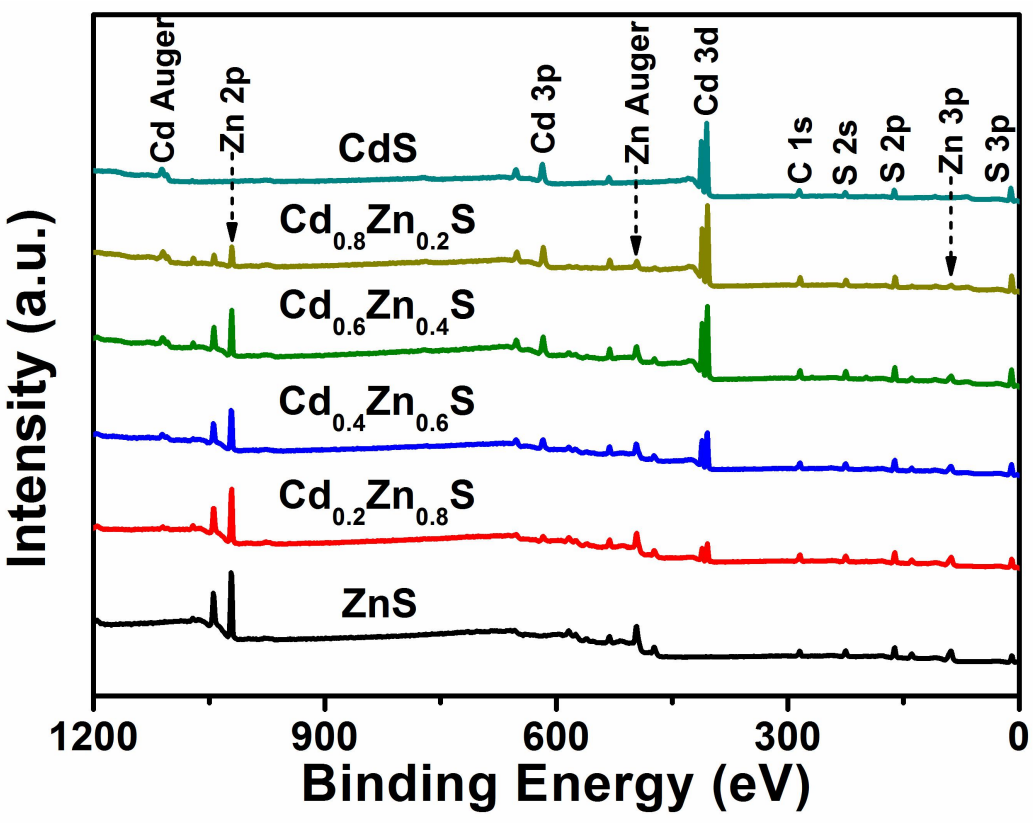
Cd Auger
Zn 2p
Cd 3p
Zn Auger
Cd 3d
C 1s
S 2s
S 2p
Zn 3p
S 3p
CdS
Cd0.8Zn0.2S
Cd0.6Zn0.4S
Cd0.4Zn0.6S
Cd0.2Zn0.8S
ZnS
Intensity (a.u.)
1200
900
600
300
0
Binding Energy (eV)

Figure S2

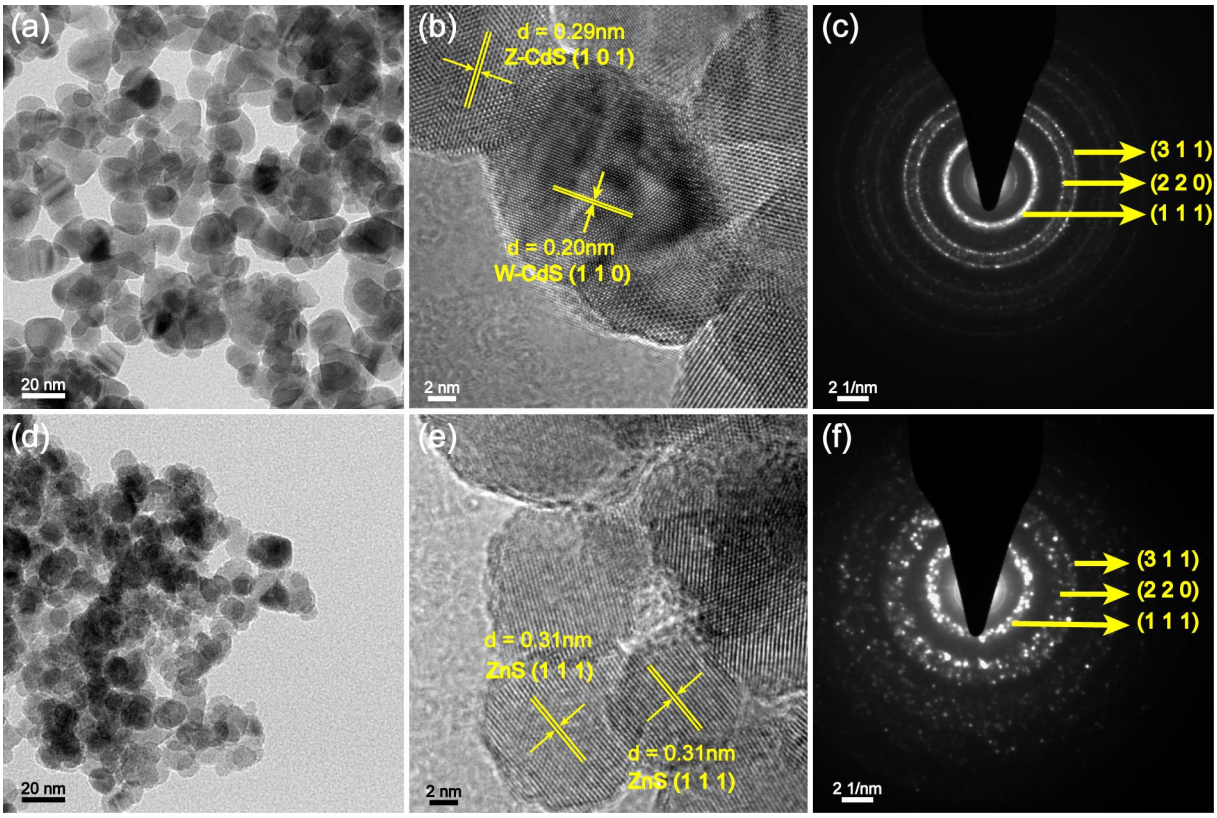
(a)
20 nm
(b)
d = 0.29nm
Z-CdS (1 0 1)
d = 0.20nm
W-CdS (1 1 0)
2 nm
(c)
(3 1 1)
(2 2 0)
(1 1 1)
2 1/nm
(d)
20 nm
(e)
d = 0.31nm
ZnS (1 1 1)
d = 0.31nm
ZnS (1 1 1)
2 nm
(f)
(3 1 1)
(2 2 0)
(1 1 1)
2 1/nm

Figure S3

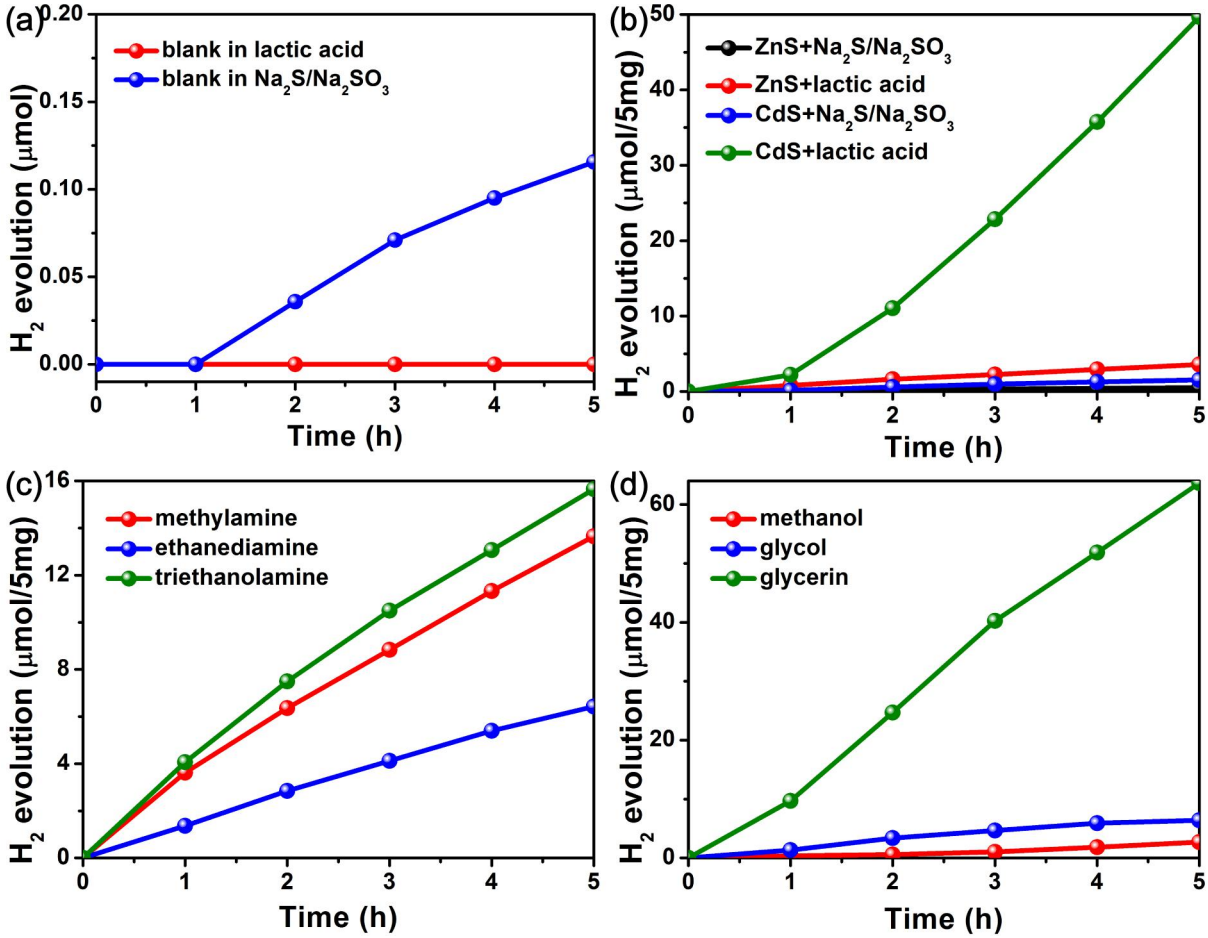
(a)
blank in lactic acid
blank in Na2S/Na2SO3
H2 evolution (μmol)
Time (h)
(b)
ZnS+Na2S/Na2SO3
ZnS+lactic acid
CdS+Na2S/Na2SO3
CdS+lactic acid
H2 evolution (μmol/5mg)
Time (h)
(c)
methylamine
ethanediamine
triethanolamine
H2 evolution (μmol/5mg)
Time (h)
(d)
methanol
glycol
glycerin
H2 evolution (μmol/5mg)
Time (h)

Figure S4

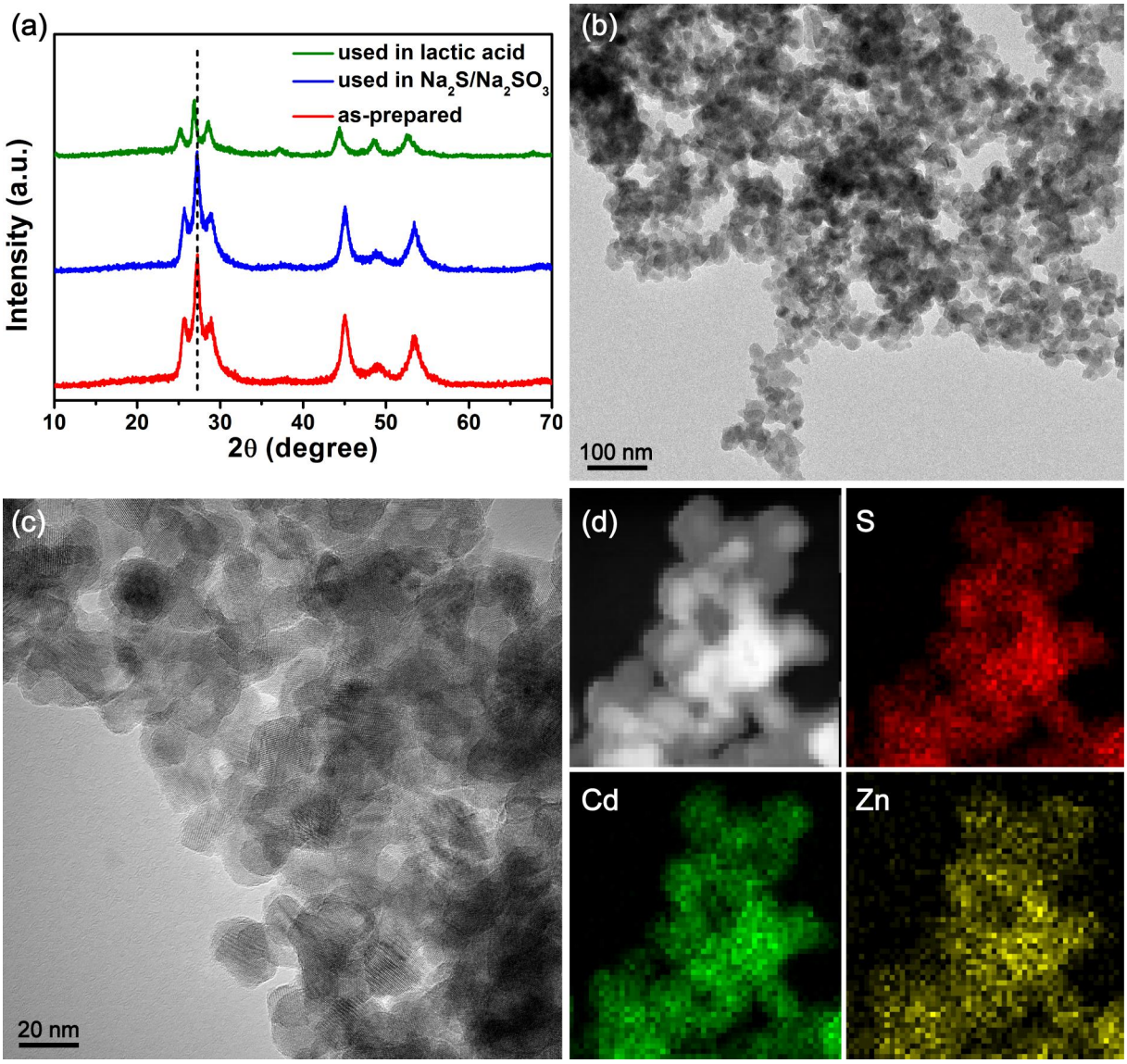
(a)
used in lactic acid
used in Na2S/Na2SO3
as-prepared
Intensity (a.u.)
10
20
30
40
50
60
70
2θ (degree)
(b)
100 nm
(c)
20 nm
(d)
S
Cd
Zn

Figure S5

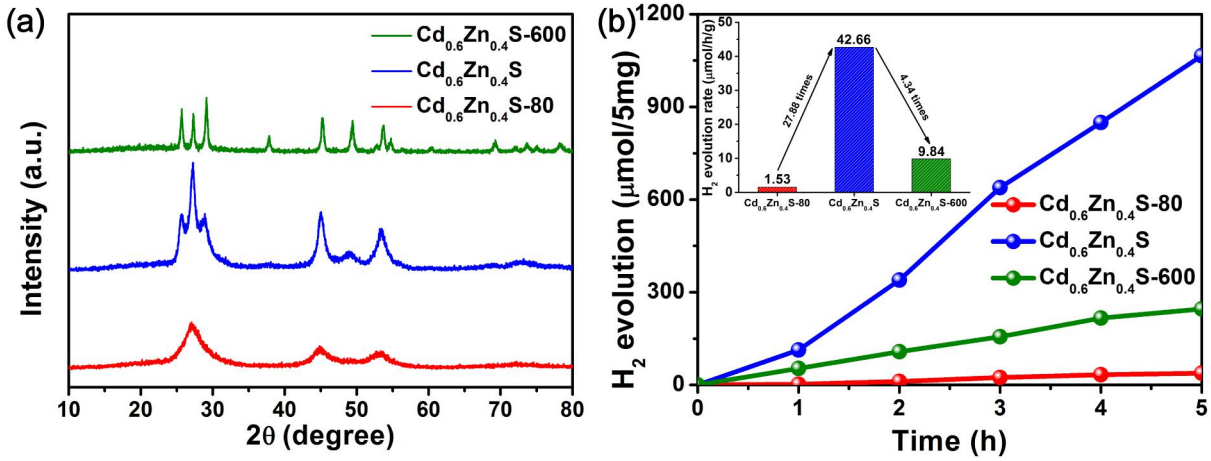

Figure S6

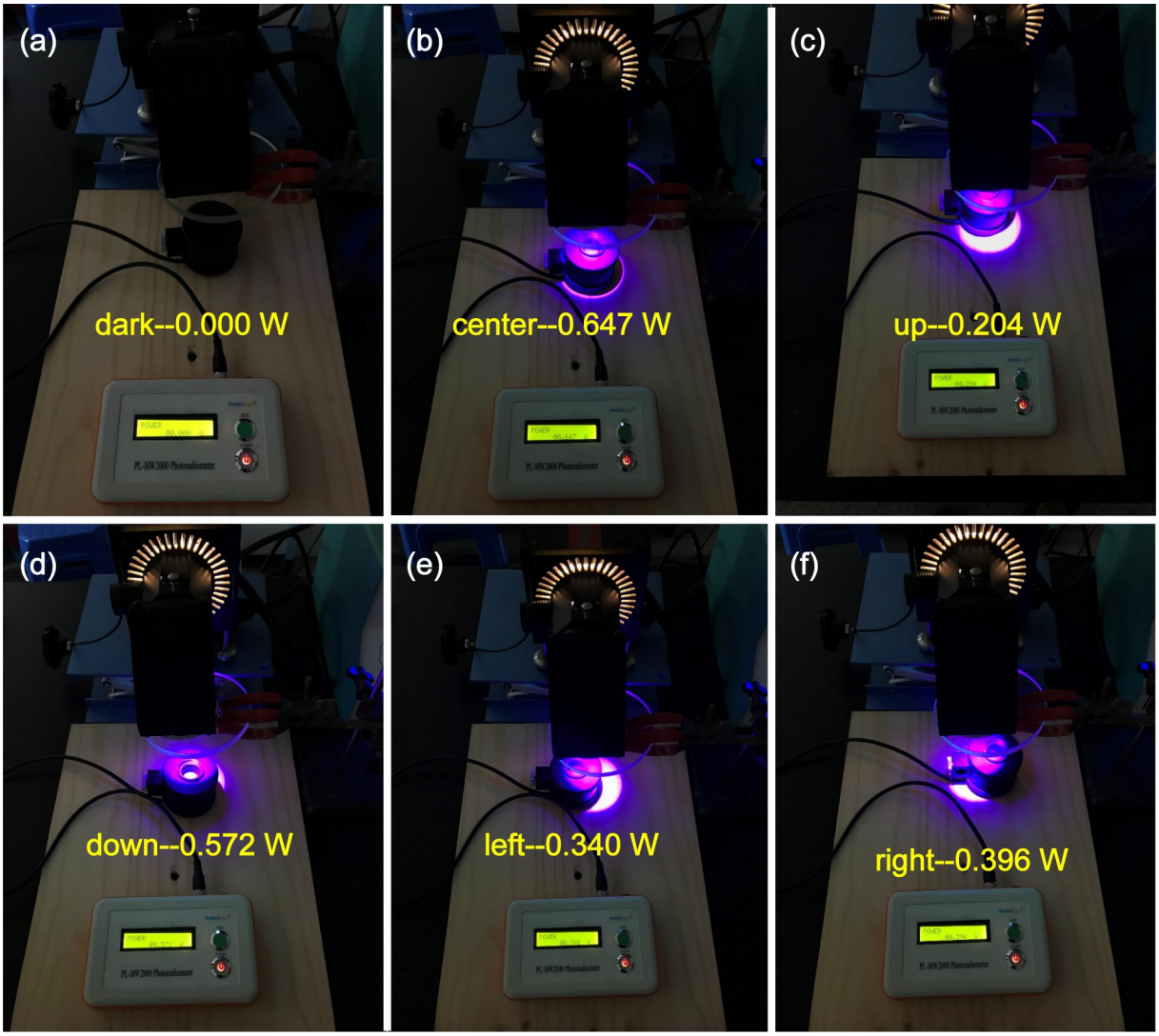

Figure S7

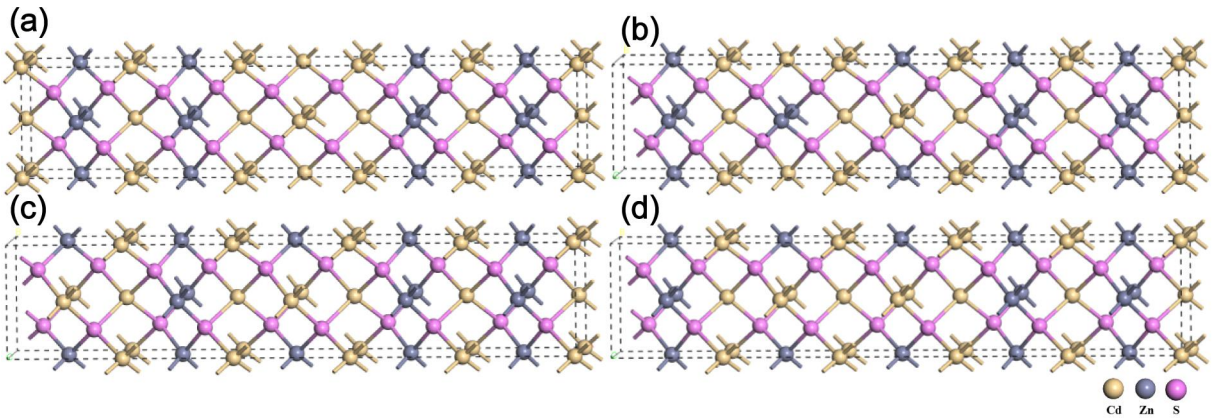

Figure S8

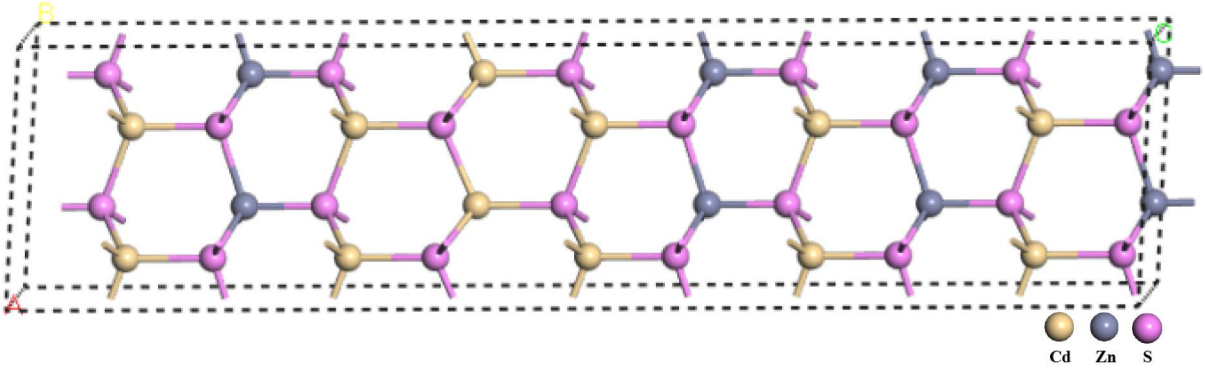

Figure S9

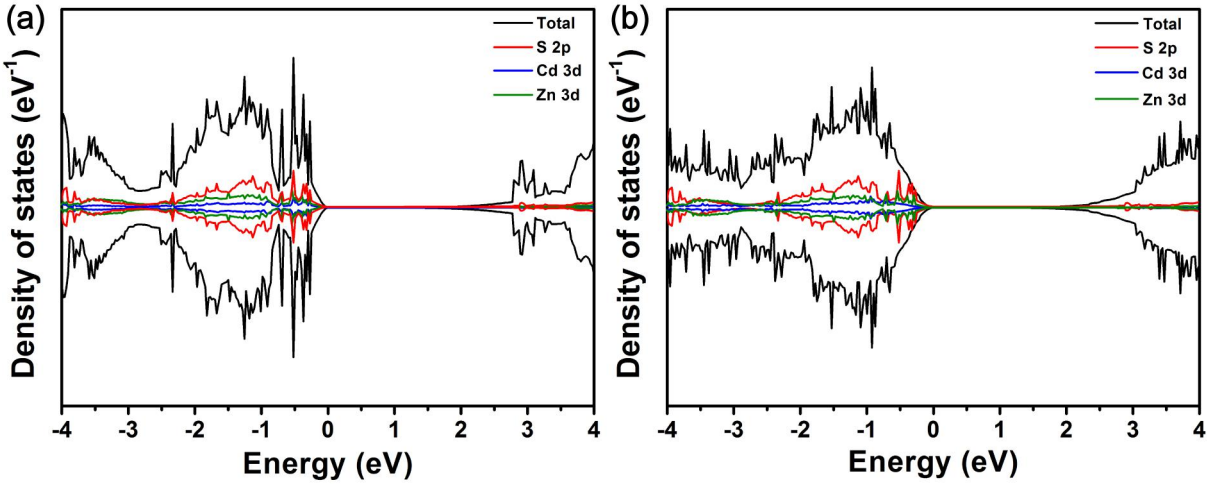

Figure S10

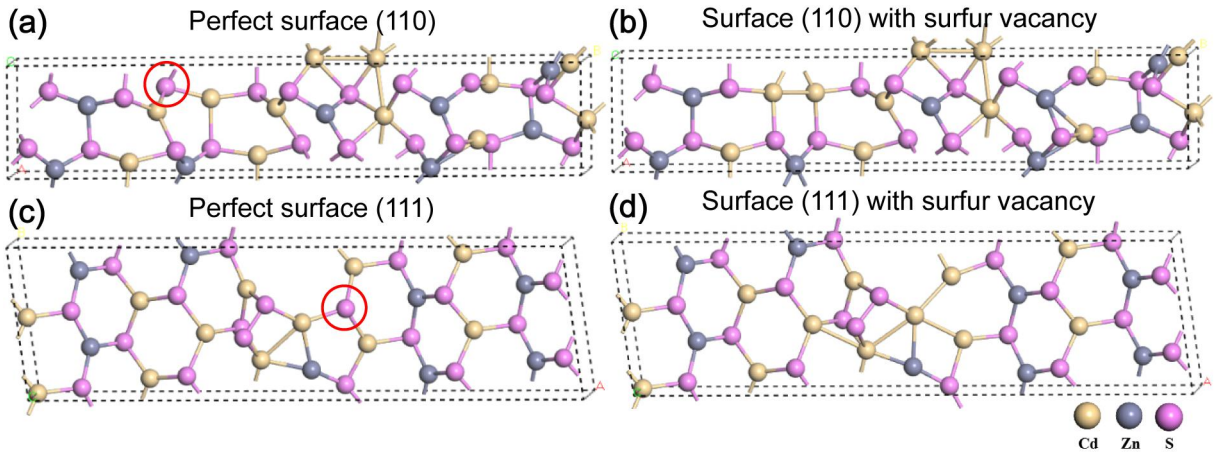

Figure S11

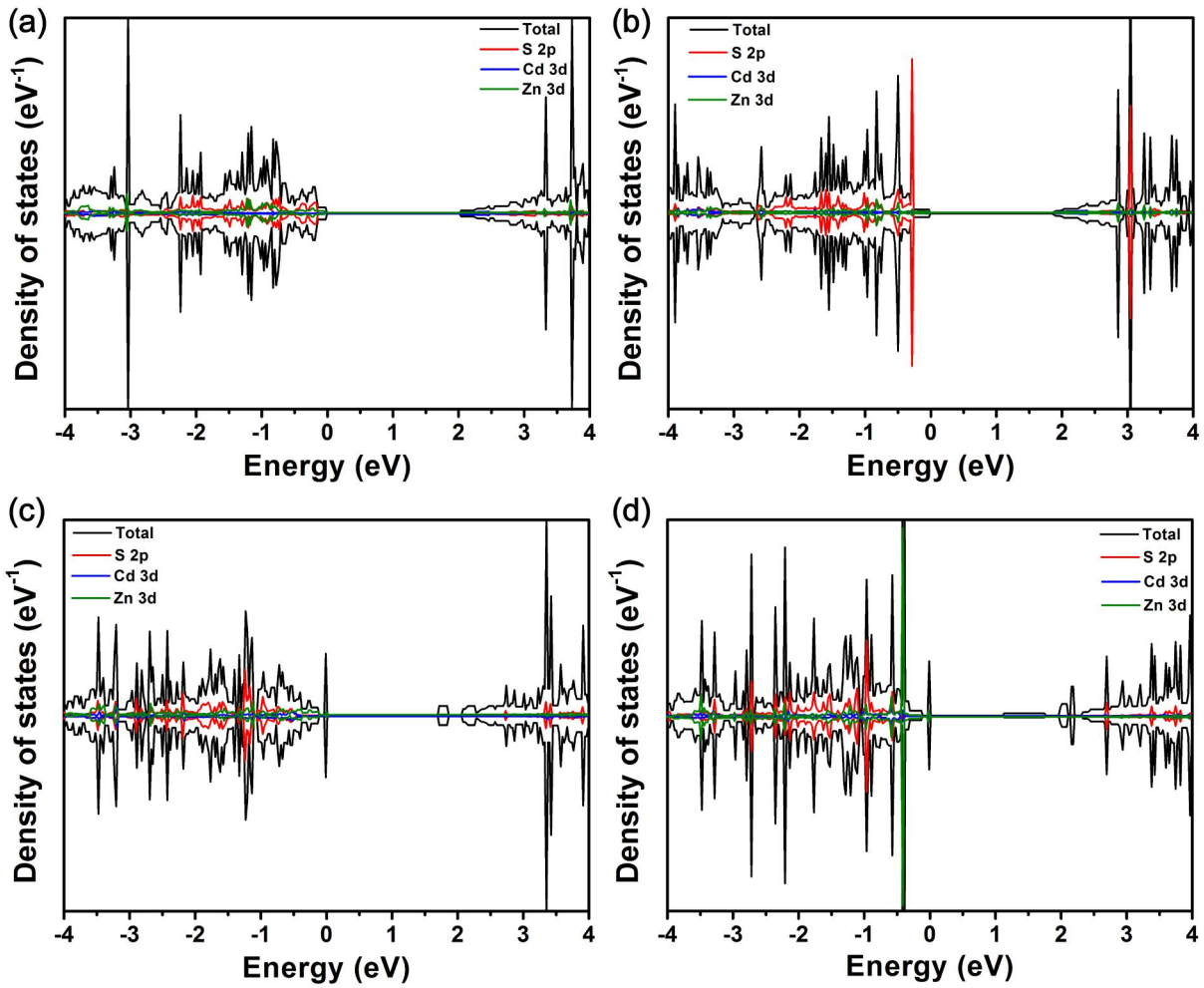

Figure S12